ELSEVIER

Journal of Molecular Catalysis A: Chemical 102 (1995) 147–161

JOURNAL OF MOLECULAR CATALYSIS A: CHEMICAL

Investigation of MoS_2 on γ-Al_2O_3 by HREM with atomic resolution

R.M. Stockmann [a], H.W. Zandbergen [b], A.D. van Langeveld [a,*], J.A. Moulijn [a]

[a] *Faculty of Chemical Technology and Materials Science, Department of Industrial Process Technology, Delft University of Technology, Julianalaan 136, 2628 BL Delft, Netherlands*

[b] *Faculty of Chemical Technology and Materials Science, National Center for High Resolution Electron Microscopy, Delft University of Technology, Rotterdamseweg 137, 2628 AL Delft, Netherlands*

Received 18 October 1994; accepted 23 May 1995

Abstract

High resolution electron microscopy and image calculations are performed on MoS_2/γ-Al_2O_3 based catalysts. It is shown that HREM allows atomic imaging of the MoS_2 particles on the alumina carrier. Restrictions with respect to atomic imaging are found from image simulations. The orientation of the slabs with respect to the electron beam is important. Whereas atomic imaging can be obtained in ⟨100⟩ and ⟨110⟩ directions, ⟨001⟩ oriented crystals will be invisible by HREM because of the way the slabs are mounted on the alumina support. The slabs are basal bounded. Since essentially single slabs are observed, it is suggested that a strong interaction exists between the slabs and the alumina support. EDX analysis shows that the MoS_2 particles are sulfur deficient. We suggest that sulfur deficiency is present in the first sulfur layer on the γ-Al_2O_3 support. In specimens sulfided below 673 K an intermediate phase is present, which is presumably an oxy-sulfide of molybdenum.

Keywords: Alumina; Atomic resolution; HREM; Molybdenum

1. Introduction

High resolution electron microscopy (HREM) is a technique which is now widely used in the characterization of catalytic materials. This is not surprising because HREM provides direct information on morphology and arrangements on an atomic scale. The newest generation of HREM microscopes now meets specifications which enables imaging with atomic resolution.

MoS_2/Al_2O_3 based catalysts are frequently used in the hydrotreatment of oil feedstock in the presence of excess hydrogen. Prior to use the oxidic catalyst is activated by sulfiding with a mixture of H_2 and sulfur containing molecules. Most often used are H_2S and thiophene. The sulfiding step is of major importance for the catalytic properties and has been extensively studied by temperature programmed sulfidation (TPS) [1,2]. Arnoldy et al. [1] evaluated a detailed reaction scheme for the sulfiding of MoO_3 on γ-Al_2O_3. The sulfiding proceeds through O–S exchange, followed by reduction of Mo(VI) to Mo(V) and Mo(IV) by rupture of Mo–S bonds with the simultaneous production of elemental sulfur. This sulfur is catalytically hydrogenated to H_2S by Mo at about 227°C. Finally, at 727 K the S/Mo ratio varies from 1.7 to 1.9 (dependent on the pre-treat-

* Corresponding author.

SSDI 1381-1169(95)00111-5

ment) thus indicating that MoS_2 particles are formed.

HREM together with EXAFS and Mössbauer spectroscopy contributed significantly in the development of a schematic picture of the active sites of hydrotreating catalysts [3–7]. These sulfided molybdenum crystallites adopt a layered hexagonal structure which shows up in the HREM micrographs as black lines. One MoS_2 layer, a so-called slab, consists of two sulfur layers with a molybdenum layer sandwiched in between and is believed to contain the active sites. The slabs can be stacked as follows: S–Mo–S...S–Mo–S...S–Mo–S. Part of the promoter atoms like Co and Ni are believed to be adsorbed on the edges of the MoS_2 slabs. The bonding between S and Mo is of a mixed ionic–covalent character whereas between the two sulfur layers of adjacent slabs only Van der Waals forces exist. Routine HREM measurements gives direct information about the average stacking height of MoS_2 slabs and their length. With these results a semi-quantitative evaluation of the HREM data is possible [3]. Insertion of the HREM statistics into a model [3,8], may provide a prediction of the relative activities of catalysts with different loading and on different alumina supports.

In this paper we report HREM results on the sulfiding of MoO_3 on different kinds of supports. It is illustrated that high resolution TEM allows imaging of the atomic arrangement of the MoS_2 slabs on γ-Al_2O_3. We draw conclusions on the slab–slab interaction in the MoS_2 and slab–support interaction. Image simulations are used to elucidate the structure of these slabs on the alumina. Some remarkable differences with the bulk structure of MoS_2 are shown and discussed.

2. Experimental

Three molybdenum catalysts were analyzed, a medium loading (A) and a high loading (B) on alumina and a high loading on zeolite YA (C).

Catalyst A was prepared by pore volume impregnation of a Ketjen CK300 000-1.5E alumina with a solution of $(NH_4)_6Mo_7O_{24}\cdot H_2O$ in water. The alumina has a BET surface area of 190 m^2/g and a pore volume of 0.60 ml/g. After vacuum evaporation, the batch was dried at 110°C for 1 h and calcined in air for 2 h at 550°C. Catalyst A was designed at 2.2 at. Mo/nm^2. We measured with atomic absorption spectroscopy (AAS) 2.0 at. Mo/nm^2.

Catalyst B was prepared by wet impregnation of a Degussa Type C alumina (median size of the primary particles 13 nm) with a solution of $(NH_4)_6Mo_7O_{24}\cdot H_2O$ in water and was designed at 36.0 wt% MoO_3. The Degussa carrier has a BET active surface of 100 m^2/g. The same drying and calcination procedure was followed as with catalyst A.

Catalyst C is a zeolite NaY in which molybdenum is incorporated, by means of deposition from Mo–hexacarbonyl. Approximately 2 Mo atoms per supercage are deposited which is about 11 wt% Mo [9].

These three catalysts were temperature programmed sulfided (TPS). For the sulfiding procedure we refer to Table 1. ϕ_v is the gas flow through the reactor.

After sulfidation all catalysts had to be exposed to air before they could be introduced into the microscope. The exposure time to air for the sulfided catalyst A was about 10 h while for catalyst B and C it was ca. 5 min.

Specimens for electron microscopy were made from a suspension of ground sample in ethanol by putting a few droplets on a holey carbon film sup-

Table 1
Sulfiding parameters for the catalysts used [1]

Catalyst	ϕ_v ml/min	$H_2S/H_2/Ar$ mixture (%)	p bar	dT/dt °C/min	T_{sulf} °C	Holding time min
A	31	3.2/24.8/72	1.2	10	250	60
					380	60
					520	60
					600	60
B	31	3.2/24.8/72	1.2	10	450	60
C	31	3.2/24.8/72	1.2	10	400	60

ported on a copper grid. For HREM analysis we used a Philips CM30 ST FEG electron microscope equipped with a field emission gun, a super twin objective lens and a CCD camera. The microscope was operated at 300 kV with a point resolution of 0.20 nm. The information limit is about 0.14 nm.

In general the specimen prepared for electron microscopy consists of separated agglomerates of γ-Al_2O_3 particles. It is important to make a proper selection of the area of a given agglomerate. We investigated only those edges of an agglomerate which are so thin that no overlap of three or more γ-Al_2O_3 particles occurs. Because of this selection, only the outer particles of Al_2O_3 agglomerates are used. Although the HREM images of the interior of the Al agglomerates are not used for the analysis they do not show significant different features. However our selection enables that straightforward conclusions can be drawn on the nature of mounting, whereas the way of mounting in the interior of the alumina region in the micrographs cannot be determined, because TEM does not carry 3-D information. Only when the surface profiling is applied, can the way of mounting be determined.

A possible cause of artifacts in the investigation of these catalysts could be their sensitivity to air. Spevack et. al. [10] concluded that the reactivity towards air depends on the stacking number of the MoS_2 slabs. Crystallites with a thickness less than 1 nm are reactive towards oxidation since they show signs of oxidation within 26 h of exposure. Spevack et. al. [10] argued that defect rich MoS_2 in contact with the support is highly reactive towards air. For this reason we kept exposure to air of catalysts B and C as short as possible (<10 min). Catalyst A was exposed overnight for 10 h. Although it is possible that exposure to air of the freshly sulfided molybdenum catalysts may influence the structures as seen by HREM, in our experience no different image features are observed when comparing samples with short exposure (<10 min) to air and those exposed to air overnight. However sulfur loss and the corresponding disintegration of MoS_2 slabs due to radiation damage is faster in samples exposed overnight. This might affect the ratio of number of slabs and spots observed. To circumvent this, illumination of the samples was kept as short as possible to prevent disintegration.

The detailed interpretation of HREM images with atomic resolution can be affected by the defocus value at which the image is formed. Especially with catalysts the defocus for various particles may vary within one image because of height variations. However, the defocus value can be estimated from experimental images. Zero defocus can be estimated from the focus at which the image contrast is minimal (ca. -20 nm). Generally, defocus values close to Scherzer defocus are used. At Scherzer focus, the microscope-induced focus shift (due to the imperfections of the objective lens) has the largest constant phase plateau which ranges from 10–0.2 nm for the electron microscope used. At Scherzer defocus, dark spots will correspond with atom positions if the specimen is sufficiently thin. For the microscope used Scherzer defocus is at -60 nm.

Image simulations were done with a simulation package MacTempas. The parameters used to simulate the Philips CM30ST FEG, are $C_s = 1.3$ mm (spherical aberration constant), $\Delta = 5.0$ nm (chromatic defocus spread) and $\theta_c = 0.1$ mrad (illumination angle).

EDX (energy disperse X-ray) analysis was performed for specimens sulfided at various temperatures. The detector was calibrated with pure MoS_2 since the sulphur $K\beta_1$ and $K\beta_x$ transitions at 2.46 keV and 2.47 keV, respectively, coincide with the $L\beta_3$ transition of molybdenum at 2.47 keV.

3. Results

3.1. MoS_2 HREM image simulations

Preliminary research indicated that the MoS_2 slabs are oriented parallel to the surface of the γ-Al_2O_3 particle as is schematically shown in Fig. 1. This generated the question how slabs which are perfectly ordered but have 'non-perfect' orienta-

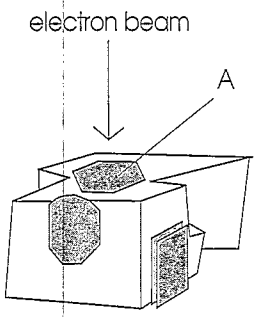

Fig. 1. Schematic model for mounting MoS_2 slabs on γ-Al_2O_3 particles.

tions (eg. tilted with respect to beam or bend) would be imaged in a high resolution electron microscope. Therefore a number of image calculations were performed:

1. The structure images for MoS_2 with the bulk structure in three different directions: ⟨001⟩, ⟨100⟩ and ⟨110⟩.
2. The effect of misalignment of the MoS_2 crystals. This is very likely to occur since the MoS_2 crystals will be oriented in all directions.
3. The effect of the support located above or below the MoS_2 crystal along the viewing direction. This is done to get a feeling for visibility of such slabs.
4. The effects of a termination of the lattice and a deviation of the stacking of the slabs.
5. Incorporation of oxygen into the MoS_2 structure.

ad 1. The structure of MoS_2 viewed in the ⟨001⟩ direction and the corresponding image simulations are shown in Fig. 2. Calculated images for various defocus values reflect the hexagonal symmetry. The HREM simulations in the ⟨100⟩ orientation show dark parallel lines perpendicular to the *c* axis, which have a distance of 0.615 nm. In these black lines narrow spacings with a distance of 0.158 nm can be observed. Although the point resolution of the microscope used is only 0.20 nm, the information limit is still sufficient to resolve the 0.158 nm spacings.

Viewing along the ⟨110⟩ direction one observes arrow-shaped image features, with a spacing of 0.274 nm. Note that at Scherzer defocus the arrow shaped image features coincide with S–Mo–S units. In the experimental image such arrows can be interpreted directly as S–Mo–S units.

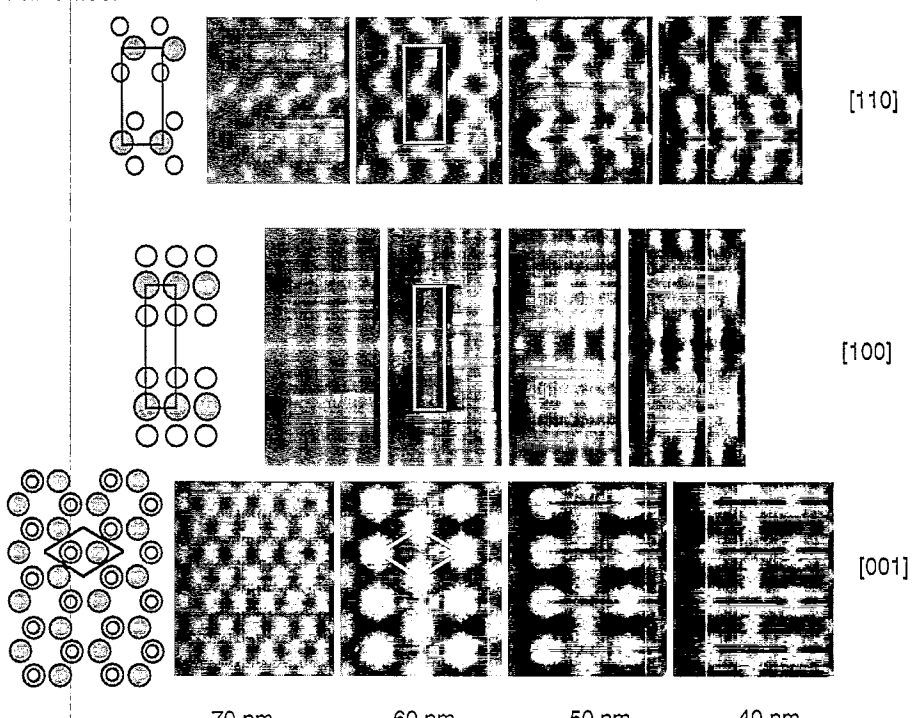

Fig. 2. Crystal structures and corresponding image simulations of MoS_2 viewed in the ⟨110⟩, ⟨100⟩ and ⟨001⟩ directions. Scherzer defocus is at −60 nm.

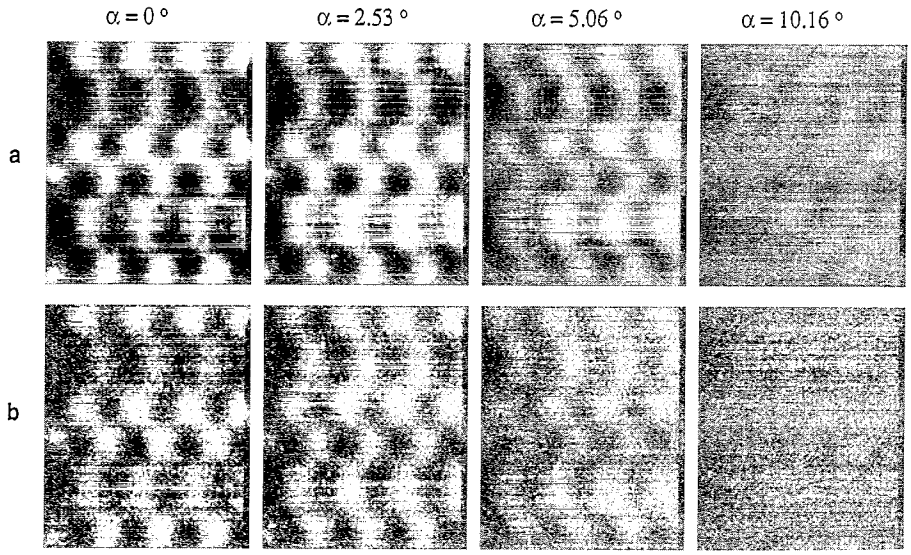

Fig. 3. Simulation of misalignment of MoS_2 slabs along the ⟨110⟩ direction. Defocus is −60 nm. The images are shown with fixed contrast. (a) 'Noise free' simulation and (b) simulation with noise added.

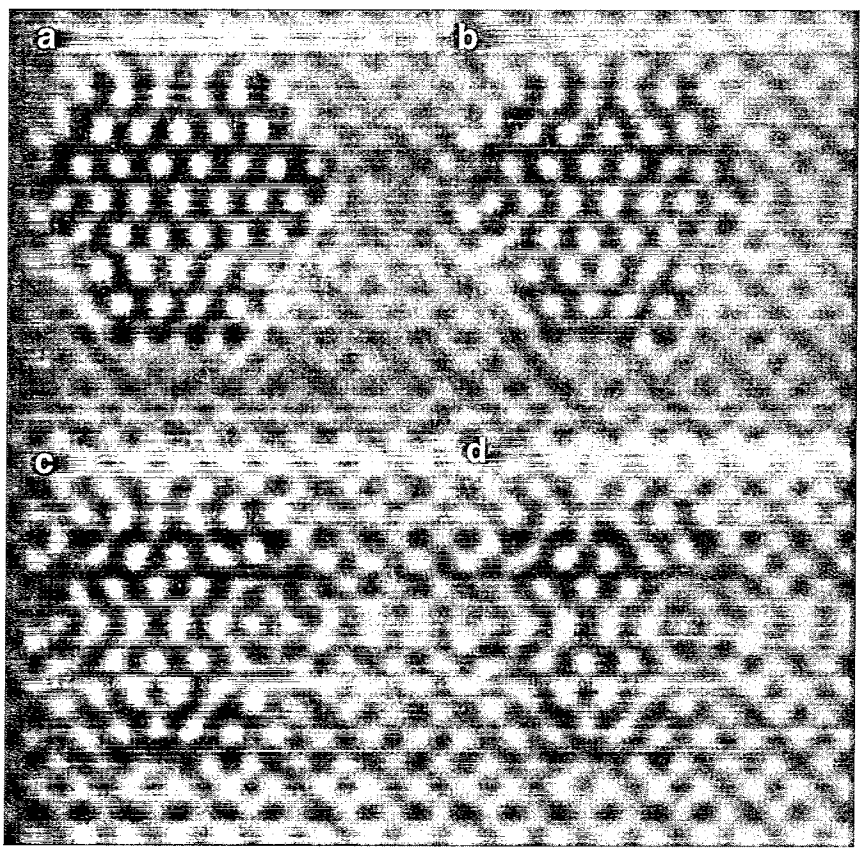

Fig. 4. Simulation of the visibility of MoS_2 slabs in the ⟨001⟩ direction on γ-Al_2O_3. The thickness of the MoS_2 is 1.2 nm and that of the γ-Al_2O_3 is 0.8, 1.6, 2.4 and 3.2 nm in a, b, c and d, respectively.

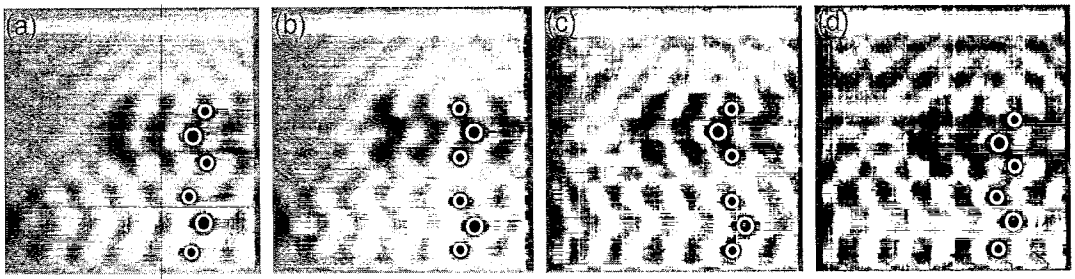

Fig. 5. Simulation of the effect of cut-off on the image of MoS_2 particles with limited length and deviations from the bulk structure. All images have been calculated for a defocus at −60 nm. (a) Bulk structure, $d_{Mo-Mo}=0.615$ nm; (b) top layer flipped, $d_{Mo-Mo}=0.615$ nm; (c) top layer shifted, $d_{Mo-Mo}=0.615$ nm; (d) arrangement as a, but with $d_{Mo-Mo}=0.57$ nm.

ad 2. A restriction for visualizing MoS_2 particles is that from all the slabs present in a certain area only a small fraction is oriented such that one of the ⟨100⟩ or ⟨110⟩ directions is parallel to the electron beam. Hence, only a few slabs will show a pattern exactly like in Fig. 2. A limit for misalignment and, therefore, visibility is obtained from image simulations. A MoS_2 slab was tilted with respect to the beam. The results are shown in Fig. 3 where for Scherzer defocus (−60 nm) different tilt angles are shown. When the sample is rotated from 0° the contrast decreases and the shape of the slabs also becomes disordered. The image blurring depends mainly on two parameters: specimen thickness and tilt of the specimen. If the thickness of the specimen along the beam is doubled then as a rule of thumb the tilt angle at which the slabs can still be resolved is halved according to the small angle approximation.

ad 3. In general the MoS_2 particles consist of 1–3 slabs with a total thickness along the *c* axis of 0.615 to 1.8 nm. In case such a MoS_2 particle

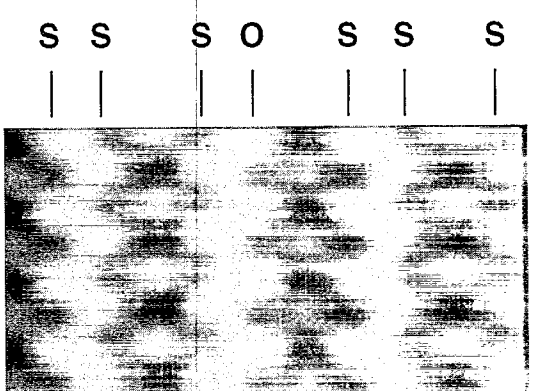

Fig. 6. The effect of substitution of sulfur by oxygen on the simulated image of the MoS_2. The various atomic layers are indicated. Note the decreased contrast at the row of oxygen atoms.

resides on a crystalline support particle like γ-alumina as the MoS_2 particle labeled 'A' in Fig. 1, the question arises how thick the γ-Al_2O_3 may be before obscuring the image of the MoS_2 slab. In order to get an idea of the 'critical thickness' of the γ-Al_2O_3, image simulations were done with a model of a 1.2 nm thick hexagonal particle oriented with its *c* axis parallel to the electron beam on top of a γ-Al_2O_3 crystal in ⟨100⟩ orientation. The thickness of the γ-Al_2O_3 support was varied from 1 to 10 nm. The results for γ-Al_2O_3 thicknesses of 0.8 nm to 3.2 nm are shown in Fig. 4. From this figure it is evident that the MoS_2 particle is only visible on a very thin (<2 nm) γ-Al_2O_3 support. Since the γ-Al_2O_3 particles we used as support vary from 3–10 nm in thickness, it can be concluded that MoS_2 particles in the ⟨001⟩ orientation will be (almost) invisible and can certainly not be discerned from thickness variations or lattice defects which also tend to occur in γ-Al_2O_3.

ad 4. The effects of slabs with a limited length as compared to bulk MoS_2, is presented in Fig. 5. Also the slab–slab distance is varied from 0.615 nm down to 0.57 nm and the orientations of the S–Mo–S positions are twisted. These simulations can be used as a reference frame when MoS_2 with a stacking of one or two is observed. In Fig. 5a to 5d some interesting features at Scherzer defocus are shown. The bulk structure as shown in Fig. 5a is in agreement with the result obtained in Fig. 2 at −60 nm. No cut-off effects are visible at the edges of the MoS_2–vacuum interface. In Fig. 5b the positions of the Mo and S atoms in the topmost slab are mirrored with respect to those in Fig. 5a.

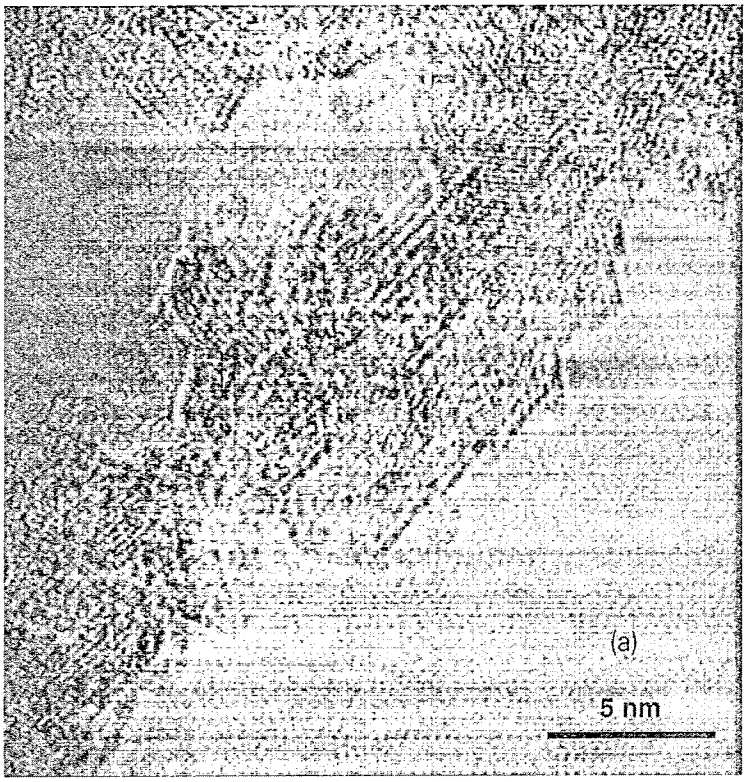
(a)
5 nm

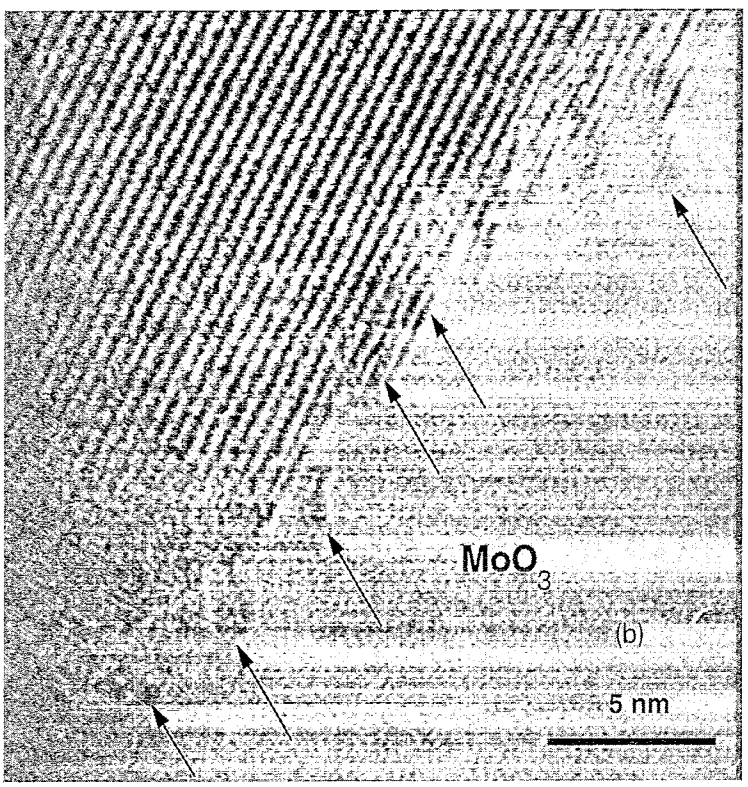
MoO3
(b)
5 nm

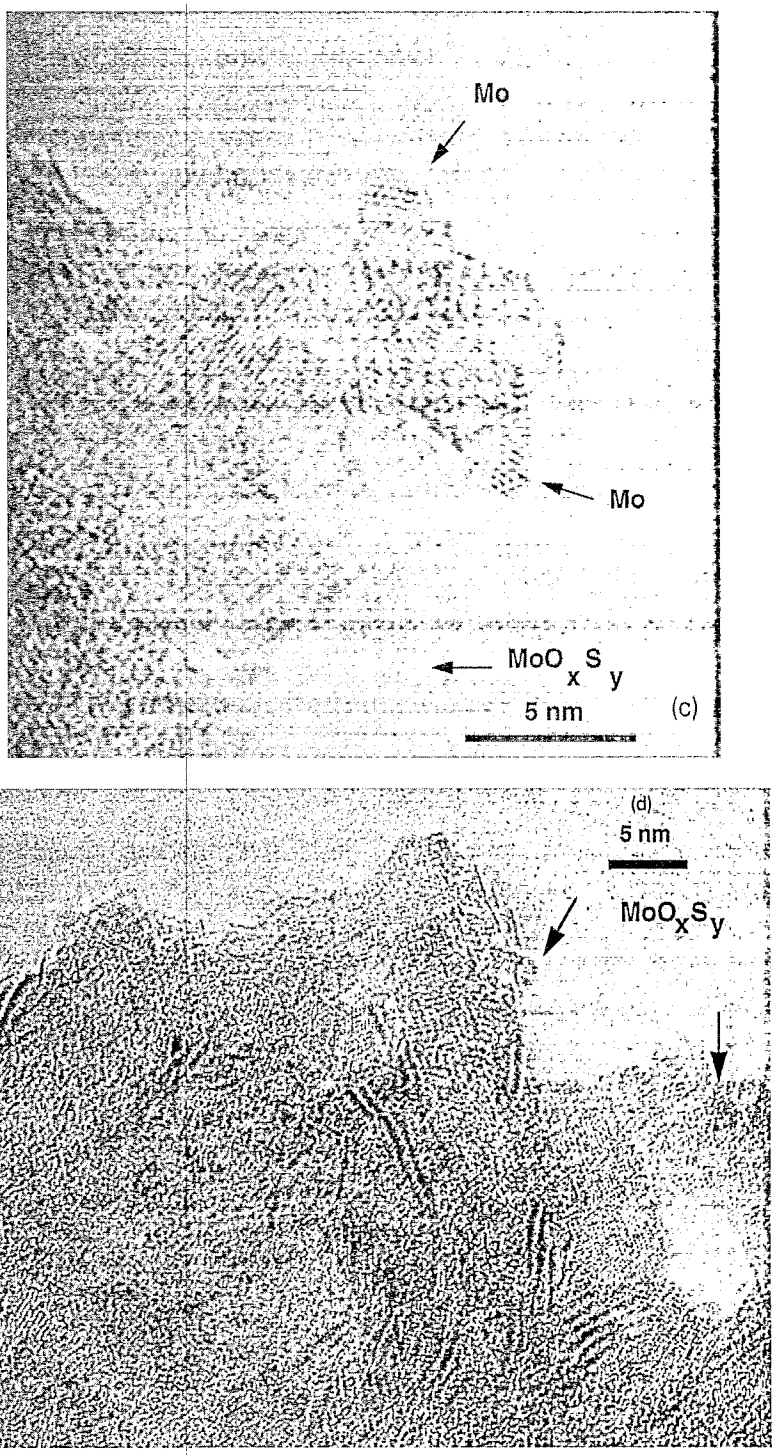

Fig. 7. (a) Bare alumina Ketjen CK300. (b) Oxidic catalyst B containing 36 wt% MoO_3. Grey dots of MoO_3 clusters are visible. (c) Catalyst A sulfided at 380°C. A mixed zone which contains both oxy-sulfides (dark spots) and MoS_2 structures (black parallel lines). Some oxy-sulfide clusters are indicated by an arrow. (d) Catalyst A sulfided at 520°C. Like in Fig. 7c, a mixed zone is shown. Note the decrease number of oxy-sulfide spots as compared to the number of MoS_2 structures.

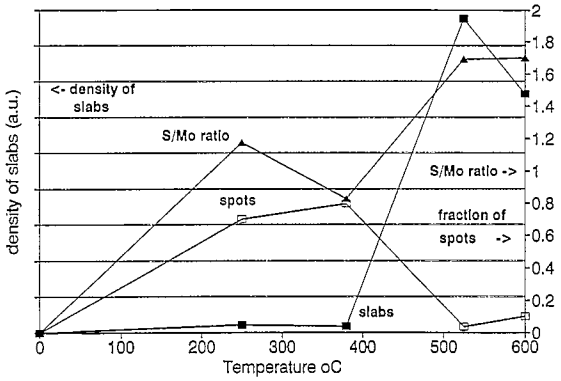

Fig. 8. Overview of the sulfiding behavior of catalyst A. The spot fraction (spots/(spots+slabs)); the slab density (a.u.) and the S/Mo ratio (determined with calibrated EDX analysis) as a function of the isothermal sulfiding temperature.

The distance between the two slabs is not changed and is still 0.615 nm (bulk value). Now the pointing direction of the arrows is flipped in the opposite direction according to the positions of the Mo and S atoms in the topmost slab. Comparing Fig. 5a and 5b at Scherzer defocus we see that the white zigzag line between the two slabs from the former figure is absent in the latter. This is due to fact that now the sulfur atoms in Fig. 5b are at the same horizontal position whereas in Fig. 5a the sulfur atoms are not aligned in this way. In Fig. 5c the topmost slab is shifted with respect to that in Fig. 5a. Fig. 5d has bulk symmetry but now the slab–slab distance is decreased from 0.615 nm to 0.57 nm. The result is that the structure image changes only slightly in this figure.

ad 5. To investigate the influence of oxygen on the structure image of MoS_2, oxygen was incorporated into the structure. One sulfur layer was replaced by an oxygen layer with a corresponding decrease in the O–Mo distance. A minor contrast difference between the oxygen and sulfur layer is visible caused by the lower scattering factor of oxygen as compared to sulfur. The O–S substitution has only a minor influence on the shape and distance of the arrow shaped image features (Fig. 6).

3.2. *The sulfiding process*

Fig. 7 a shows a HREM image of the bare Ketjen alumina. Loading this support with MoO_3 up to monolayer coverage (about 2.5 at. Mo/nm^2) does not significantly change the HREM images. Only at higher loadings, significant differences with the bare carrier are visible: (i) large separate MoO_3 particles (>10 nm) and (ii) small dark spots on the γ-Al_2O_3 carrier (see Fig. 7b).

In the sulfided catalyst black parallel lines of the MoS_2 slabs are visible. With catalyst A mostly single slabs are observed. The lengths of the slabs are between 1 to 5 nm. Sometimes double slabs are observed with a variable slab–slab distance of 0.57 to 0.62 nm. This distance must be treated with care as will be discussed. Catalyst B shows mostly double and triple stacked slabs in accord with the higher loading per surface area. The slab length is roughly the same as that in catalyst A.

In the specimen sulfided at intermediate temperatures (200 to 400°C in Fig. 8), dark spots occur which are only clearly visible in the very thin parts of the agglomerates of alumina particles (Fig. 7c and 7d). They are most likely also present in the thicker regions but cannot be distinguished. Regions (size between 100 nm to 250 nm in diameter) with only slabs, only spots and a mixture of slabs and spots (majority) are observed. Between the slab-rich and spot-rich regions, there are regions with both spots and slabs.

In the spots sometimes lattice fringes could be observed which were rapidly showing up and disappearing, indicating a fast change in orientation. The spacings observed correspond to those of metallic Mo. Such a rapid change in orientation has been reported previously for small metal particles [11]. This indicates that upon exposure to the electron beam some particles become metallic (Mo).

A statistical analysis of the density of slabs, the spot/slab ratio and the S/Mo ratio as a function of the sulfidation temperature is presented in Fig. 8. At intermediate sulfiding temperatures (200°C–400°C) a low density of slabs and a high density of spots is observed. At sulfiding temperatures above 400°C the slab-density is high and correspondingly the spot density is low. EDX analysis (averaged over many areas) of samples sulfided at temperatures between 200°C and

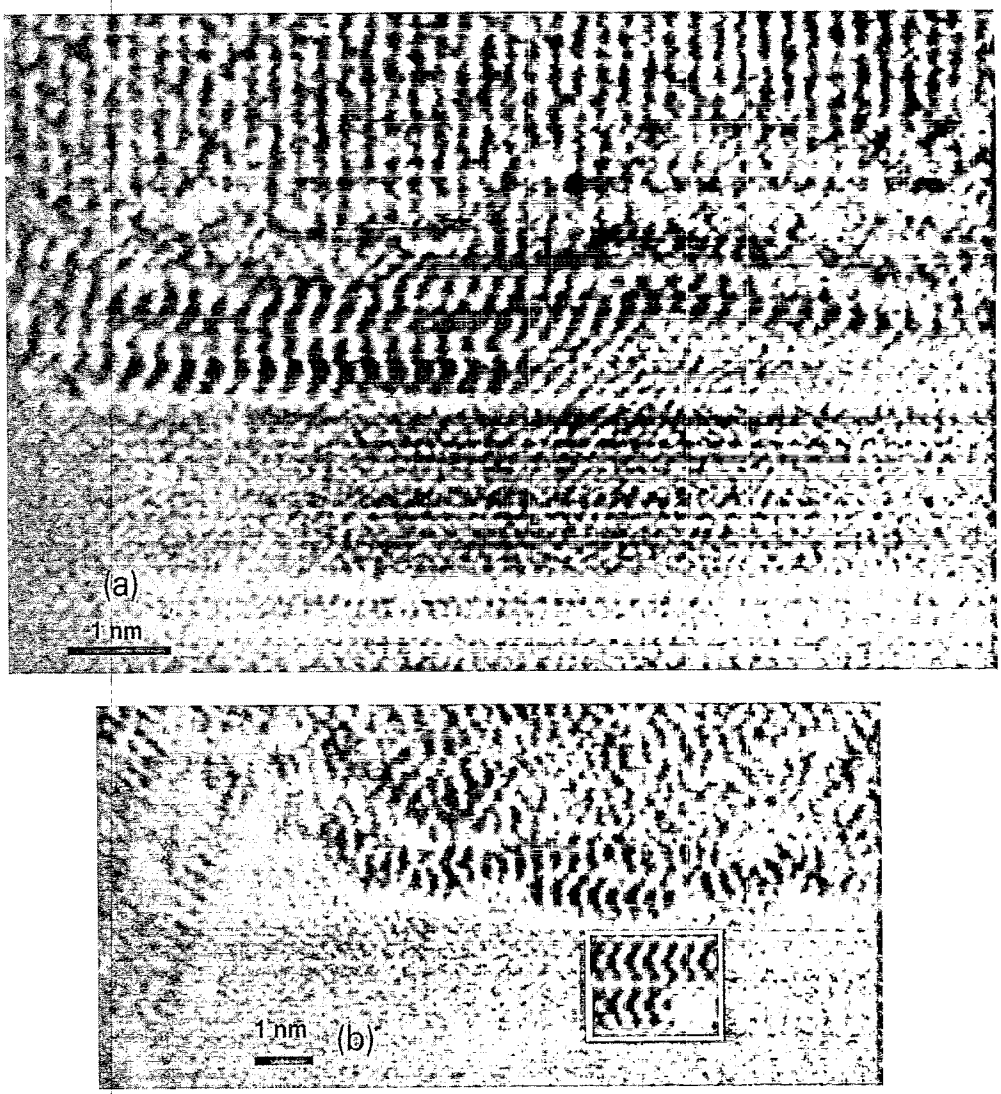

Fig. 9. (a) Catalysts B sulfided at 450°C. Two MoS_2 slabs on top of the alumina can be observed. Note that the image features do not correspond to those of bulk MoS_2. (b) Catalysts B sulfided at 450°C. As in Fig. 9a, two slabs on top of the alumina are shown. Here, the image features match perfectly those of bulk MoS_2. However, this is only rarely observed.

400°C showed that the S/Mo ratio is around 1 and after sulfidation above 400°C it is about 1.7. This indicates that the Mo is incompletely sulfided at all temperatures. The standard deviation of the S/Mo ratio for a series of measurements of the same area is less than 10%. Since the S/Mo ratios are averages it is likely that the 300°C sample contains MoS_2 slabs with composition 1.7 or less and MoS_xO_y with low x.

3.3. Structure of MoS_2 slabs on alumina

In Fig. 9a and 9b two slabs on an alumina particle are shown. From the spacing within one slab we infer that the slabs are in ⟨110⟩ orientation. However, the observed experimental pattern is different from that in the simulations where the S–Mo–S arrows of two adjacent layers point in opposite directions. In Fig. 9a this image feature is not present, indicating that the structure of MoS_2 slabs on alumina is different from that of the bulk. In Fig. 9b also a double slab on an alumina particle is shown with a focus setting below Scherzer defocus. If we compare Fig. 9b with the simulation at −80 nm defocus (see inset in Fig. 9b) we can identify the same image features for the top slabs in both the experimental image and simulation. In

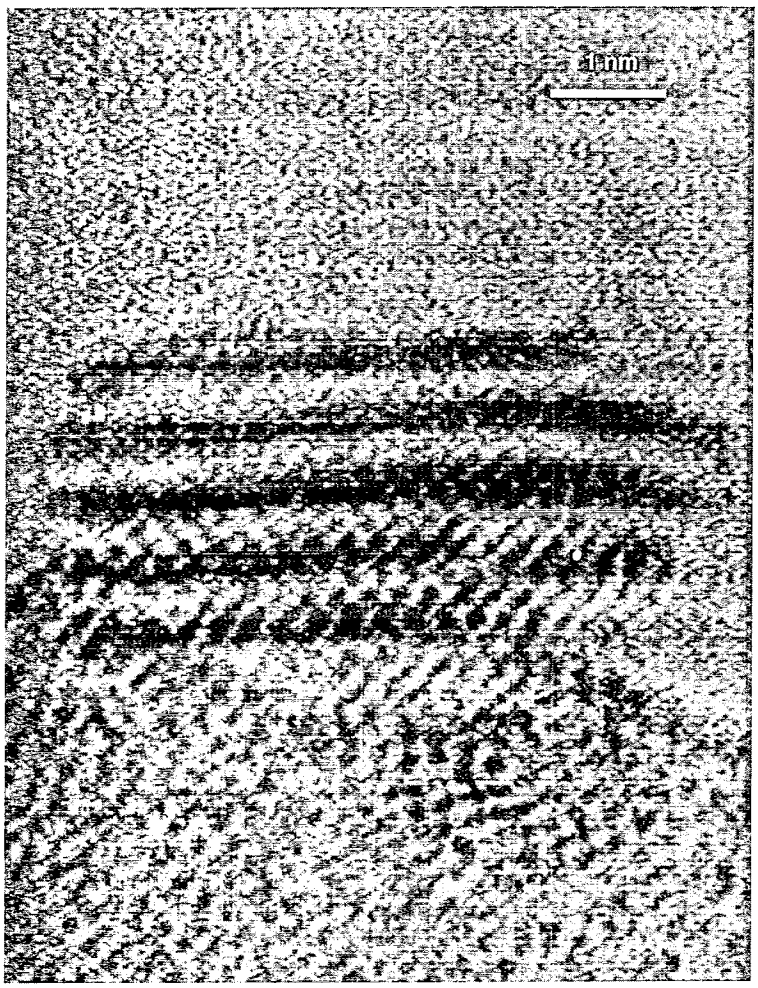

Fig. 10. Catalysts B sulfided at 450°C. Stacking of 5 MoS_2 layers is shown. The two slabs next to the alumina have the ⟨110⟩ orientation, whereas the topmost three slabs do not show detailed features corresponding to atomic imaging.

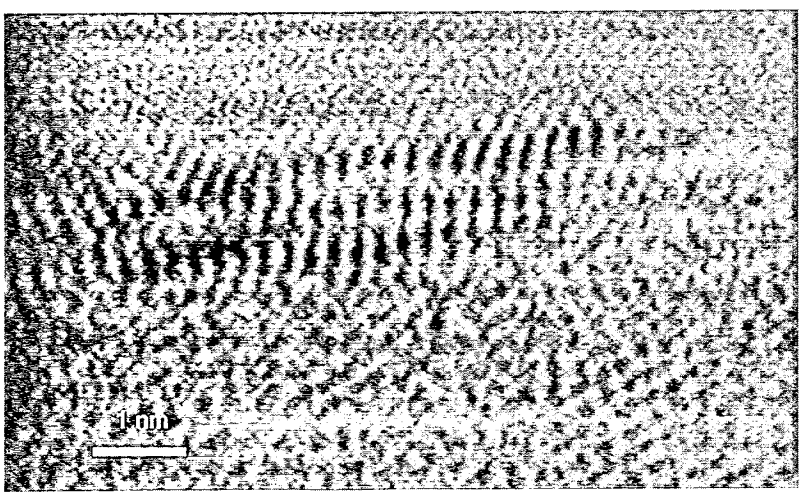

Fig. 11. Catalysts B sulfided at 450°C. An example of a dislocation where two slabs are partly intercalated by a third slab –a phenomenon which is regularly observed.

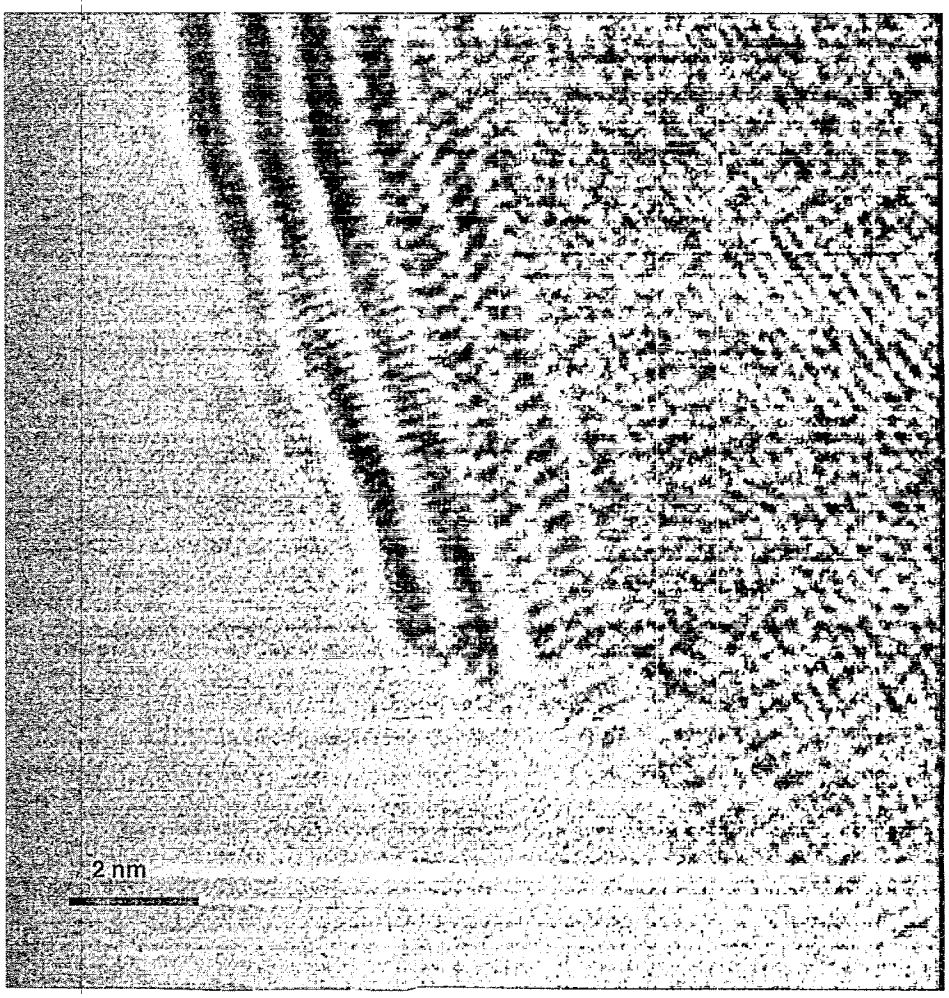

Fig. 12. Stacking of 5 to 6 MoS_2 slabs as observed on catalyst C. Both the ⟨100⟩ and the ⟨110⟩ orientations are observed in the slab, thus suggesting that the slabs are rotated by 30° with respect to each other.

both cases we see that an arrow has been transformed into a black spot (marker 1 and 1′). Hence, we can conclude in this rather exceptional case that the agreement between experimental and theoretical results is quite good.

In Fig. 10 one can observe a stacking of 5 slabs on the alumina surface. In this case the two bottom slabs show the ⟨110⟩ orientation, whereas the three slabs on top show no intra-slab image features. The loss of image features is probably related to a rotation of the 3 top layers such that no structure in the slab can be seen. We also frequently observe dislocations in the MoS_2 particles. A typical example is given in Fig. 11: between two slabs a third slab appears.

To acquire a good understanding of the slab–slab stacking and the slab–slab interaction we also analyzed MoS_2 on zeolite YA (C), which was selected because of its high stacking number of the slabs and its similar sulfiding procedure. A HREM image of a stack of 5 MoS_2 slabs on top of a zeolite is shown in Fig. 12a, which is enlarged in 12b. In Fig. 12b one can observe that the MoS_2 crystallite contains two different orientations due to rotation of the topmost part by 30° around its *c* axis. This feature was observed frequently.

4. Discussion

4.1. Image simulations

The image simulations of the 1.2 nm thick hexagon shaped MoS_2 particle on top of ⟨100⟩ ori-

ented γ-Al_2O_3 showed that the MoS_2 will not be or hardly visible when the γ-Al_2O_3 is thicker than 4 nm. In this respect one has to take into account that a disorientation of the γ-Al_2O_3 results in a better visibility of the MoS_2 particle and that on the other hand a disorientation of the MoS_2 particle will decrease its visibility. The HREM images show that the γ-Al_2O_3 particles have a thickness in the range of 3 to 15 nm. This agrees with the average thickness as calculated with a formula reported by Kerkhof and Moulijn [12]:

$$t = 2/(\rho_s \cdot S_0)$$

where t is the thickness (m) ρ_s the density (g/m^3) and S_0 is the specific surface (m^2/g). If we use the values for catalyst A we obtain $t = 11$ nm, in agreement with the EM results. The image calculations show that for such a thickness of γ-Al_2O_3 the double MoS_2 slab cannot be identified any more.

The image calculations show that the possibility of imaging the atomic structure depends strongly on the orientation of the slabs with respect to the electron beam. The best results are obtained for slabs in the exact ⟨100⟩ or ⟨110⟩ orientation. Small deviations up to about 3° from these orientations lead to a decreased contrast and loss of symmetry, but interpretation on an atomic scale is still possible. For greater deviations the loss, by contrast, will result in detection problems and the interpretation will be complicated. This is quite understandable because the HREM images provide in first approximation an image of the projection of the structure; a tilt from an orientation along a column of atoms will result in a blurred image.

Apart from the disorientation of the MoS_2 crystal to the electron beam also the support is a source for decreased visibility. Because of the manner in which the MoS_2 particle is mounted on the support, atomic imaging of ⟨001⟩ oriented MoS_2 will not be possible because of blurring by the underlying support. Furthermore, since the curvature of the MoS_2 slab is governed by the support, the MoS_2 particle will often be bent, leading to additional blurring of the structure image.

Although the image of the MoS_2 will be blurred or invisible, in the main, one should still be able to image a significant fraction of the of slabs with a structure image very similar to those of the image calculations. However, this is not found experimentally; the fraction of slabs which show the bulk-like structure image is very scarce. This indicates that the structure of the MoS_2 particles on top of the γ-Al_2O_3 support is not as perfect as that of bulk MoS_2.

4.2. *The sulfiding process*

The dark spots ranging in size from 1.5 to 3 nm (see Fig. 7c and 7d) are probably an intermediate oxy-sulfide. Several checks have been performed to assure that these spots are not an artifact. First, the bare carrier was sulfided at 350°C, to check whether this results in spots on the γ-Al_2O_3. This was not the case. Second, a check was made in which catalyst A was exposed to an heat treatment in argon at 350°C; no spots were observed. Third, EDX analysis on areas in the sulfided materials having only these dark spots showed in the presence of S and Mo but with a low S/Mo ratio. From this we conclude that the spots are indeed related to a molybdenum phase. Both the Mo/S ratio and the absence of MoS_2 slabs indicate that these dark spots consist of a partially sulfided phase.

The observation of slab–slab distances ranging from bulk distance to somewhat lower values (0.615 nm–0.57 nm) is quite remarkable. The smaller distances can very well be an artifacts due to the imperfect structure of the MoS_2 slabs. In the case of perfect slabs one can take the middle of the black MoS_2 lines as the position of the Mo atoms. But as we have seen, misalignment, oxygen incorporation and defects will result in a image in which the symmetry is lost, such that the Mo atoms can no longer be pinpointed. In that case the middle of the black lines does not have to correspond to the Mo positions resulting in a 'measured' slab–slab distance which differs from the actual value. The measured slab–slab distances in the double and triple slabs are in general shorter than the bulk values. This suggests that the posi-

tions of the outer Mo layers do not coincide with those in the middle of the slab. Possibly, this is due to vacancies in the S layer exposed to the vacuum. S → O exchange might also be considered but according to Fig. 6 this would not lead to the apparent contraction of the Mo layers, since oxygen shows similar darkening to that of the sulfur atoms.

From the EDX measurements it was concluded that between 400°C and 600°C the S/Mo ratio is about 1.7. This suggests that there are still quite a number of Mo–O bonds. The most likely position of these oxygens in MoS_2 slabs is in the bottom layer located on top of the alumina surface. In general the slab mounted on the alumina surface has an irregular structure (see Fig. 9a and 9b) which can be related to incorporation of O in the sulfur layer. The oxygen in the oxy-sulfide has of course no preferable position if we assume that MoO_xS_y has an amorphous structure. Our results with respect to the S/Mo ratio are in agreement with Kemp et al. [13] who concluded from XPS data that approximately 15–20% of the molybdenum is bonded to residual oxygen. This is also put forward by Delannay [14] who suggested an oxy-sulfide to be present next to stoichiometric MoS_2. This is in good agreement with our observations of both oxy-sulfides (spots) and MoS_2 (slabs) on the same catalyst. The molybdenum oxy-sulfide is apparently unstable in the electron beam, and reduces into metallic Mo particles. In contrast, the MoS_2 slabs are reasonably stable in the electron beam. The existence of Mo–O bonds after completion of the sulfiding process is in agreement with the sulfiding scheme of Arnoldy et al. [1].

4.3. Mounting of the slabs on the alumina

We conclude that the MoS_2 particles are only basal bonded. This is agreement with Van Doorn et al. [15] who proposed a morphological model of an alumina supported NiMo catalyst in the working state. Hayden et al. [4] claimed that the MoS_2 slabs can either be basal bonded to the alumina surface or edge bonded. However, in our study only one out of thousands slabs was observed to be edge bonded. The results of Hayden et al. [4] can be explained in the following way. The authors grew a homogeneous amorphous layer of Al_2O_3 on Al by etch oxidation. Successive annealing to γ-Al_2O_3 in O_2 at 870 K for about 90 ks was performed which must have resulted in the formation of micropores. We suggest that the black lines observed in the HREM images, suggested by the authors to be due to edge bonding, are actually basal bonded MoS_2 particles located in the pores.

The MoS_2 slabs are very flexible towards bending without losing their layered structure. The ultimate example of bending is that recently closed cages of MoS_2 are reported, analogous to the C_{60} fullerenes (buckyballs) [16].

The sulfur deficiency can be explained by an incomplete substitution of oxygen by sulfur. During sulfiding not all of the Al–O–Mo linkages are broken, thus introducing slabs with defects in the sulfur layer on top of the alumina surface. If the bottom sulfur layer had no defects, only weak Van der Waals forces would be present between slabs and the alumina. However, the experimental results (Fig. 7 and Fig. 9) suggest that the bottom sulfur layer is fairly strongly bonded with the alumina, indicating the presence of another type of interaction than that of Van der Waals between the MoS_2 and the alumina.

4.4. Structure of MoS_2 slabs on alumina

In Fig. 12a and 12b slabs with five-fold stacking mounted on zeolite (YA) are shown. From this micrograph we see that the slabs are positioned on each other with a different orientation: ⟨110⟩–⟨110⟩–⟨100⟩–⟨100⟩–⟨100⟩. This means that the existing Van der Waals forces are too weak to produce a regular structure under the conditions at which the stacked slabs were formed. On the alumina we observe a similar phenomenon. Fig. 10 shows a stacking of five MoS_2 slabs on alumina but in this case the dark lines of the topmost 3 slabs show no structure features indicating that these slabs are rotated for an angle between 5 and 25° around the *c* axis, since a rotation over

$30 \pm 5°$ would give these details as shown in Fig. 12a. Because of the closed packed stacking of the sulfur layers on top of each other, angles of 0 and $n\pi/3$ would give maximum interaction between the layers. A deviating angle will result in a decreased Van der Waals interaction. The frequent observation of a tilt of 30° in the zeolite sample indicates a small energy minimum for this orientation.

Dislocations in the slab layers are frequently observed on all carriers and can, again, be attributed to the generally weak Van der Waals interaction between the slabs.

5. Conclusions

1. Atomic imaging gives useful information on the atomic arrangement in the MoS_2 particles.
2. Image simulations show that the visibility and the loss of symmetry depends strongly on the orientation of the MoS_2 particles with respect to the electron beam.
3. Slabs are basal bonded on the alumina surface.
4. On alumina mostly single slabs are present, indicating a slab–alumina interaction which is considerably stronger than the slab–slab interaction.
5. Very few 'perfect' crystals are observed, indicating that the MoS_2 crystals contain many defects like curvature of the slabs, sulfur vacancies, substitution of sulfur by oxygen and dislocations.
6. The MoS_2 particles are sulfur deficient. The most likely location for the sulfur deficiencies is the first sulfur layer on the γ-Al_2O_3 support where oxygen atoms occupy sulfur positions.
7. An intermediate phase, presumably an oxy-sulfide of Mo, is formed at sulfiding temperatures below 400°C.

Acknowledgements

These investigations were supported by the Netherlands Foundation for Chemical Research (SON) with financial aid from the Netherlands Technology Foundations (STW). We would like to thank Dr. W.J.J. Welters and Ir. Vissenberg (Eindhoven University of Technology) for providing catalyst C. Ir. J.P. Janssens (Delft University of Technology) is gratefully acknowledged for his assistance with the temperature programmed sulfiding.

References

[1] P. Arnoldy, M.C. Franken, B. Scheffer and J.A. Moulijn, J. Catal., 92 (1985) 35.
[2] J.A. Moulijn, P.W.N.M. van Leeuwen and R.A. van Santen, Catalysis: An Integrated Approach to Homogeneous, Heterogeneous and Industrial Catalysis, Netherlands Institute for Catalysis Research, Elsevier, Amsterdam, 1993.
[3] S. Eijsbouts, J.J.L. Heinerman and H.J.W. Elzerman, Appl. Catal. A, 105 (1993) 53 and 69.
[4] T.F. Hayden and J.A. Dumesic, J. Catal., 103 (1987) 366.
[5] S.M.A.M. Bouwens, R. Prins, V.H.J. de Beer and D.C. Koningsberger, J. Phys. Chem., 94 (1990) 3711.
[6] W. Niemann, B.S. Clausen and H. Topsoe, Catal. Lett., 4 (1990) 355.
[7] C. Wivel, R. Candia, B.S. Clausen, S. Morup and H. Topsoe, J. Catal., 68 (1981) 453.
[8] S. Kasztelan, H. Toulhoat, J. Grimblot and J.P. Bonnelle, Appl. Catal., 13 (1984) 127.
[9] W.J.J. Welters, Thesis, Eindhoven University of Technology (1994)
[10] P.A. Spevack and S. McIntyre, Appl. Catal., 64 (1990) 191.
[11] Wallenberg, NCHREM Sweden, private communication.
[12] F.P.J.M. Kerkhof and J.A. Moulijn, J. Phys. Chem., 83 no. 12 (1979) 1612
[13] R.A. Kemp, R.C. Ryan and J.A. Smegal, in M.J. Phillips and M. Ternan (Eds.), Proc. 9th Int. Congress on Catalysis, Vol. 1, Calgary, 1988, p. 128.
[14] F. Delannay, Appl. Catal., 16 (1985) 135.
[15] J. van Doorn, J.A. Moulijn and G. Djéga-Mariadassou, Appl. Catal., 63 (1990) 77.
[16] W. Kratschmer, Europhysics News, 24 no. 9 (1993) 220.